

Single particle tracking reveals spatial and dynamic organization of the *Escherichia coli* biofilm matrix

This content has been downloaded from IOPscience. Please scroll down to see the full text.

2014 New J. Phys. 16 085014

(<http://iopscience.iop.org/1367-2630/16/8/085014>)

View [the table of contents for this issue](#), or go to the [journal homepage](#) for more

Download details:

IP Address: 18.51.1.3

This content was downloaded on 14/10/2014 at 14:13

Please note that [terms and conditions apply](#).

Single particle tracking reveals spatial and dynamic organization of the *Escherichia coli* biofilm matrix

Alona Birjiniuk¹, Nicole Billings², Elizabeth Nance³, Justin Hanes³, Katharina Ribbeck² and Patrick S Doyle¹

¹ Department of Chemical Engineering, Massachusetts Institute of Technology, Cambridge, MA 02139, USA

² Department of Biological Engineering, Massachusetts Institute of Technology, Cambridge, MA 02139, USA

³ Center for Nanomedicine at the Wilmer Eye Institute, Johns Hopkins University, Baltimore, MD 21231, USA

E-mail: pdoyle@mit.edu and ribbeck@mit.edu

Received 28 February 2014, revised 25 April 2014

Accepted for publication 2 June 2014

Published 27 August 2014

New Journal of Physics **16** (2014) 085014


doi:[10.1088/1367-2630/16/8/085014](https://doi.org/10.1088/1367-2630/16/8/085014)

Abstract

Biofilms are communities of surface-adherent bacteria surrounded by secreted polymers known as the extracellular polymeric substance. Biofilms are harmful in many industries, and thus it is of great interest to understand their mechanical properties and structure to determine ways to destabilize them. By performing single particle tracking with beads of varying surface functionalization it was found that charge interactions play a key role in mediating mobility within biofilms. With a combination of single particle tracking and microrheological concepts, it was found that *Escherichia coli* biofilms display height dependent charge density that evolves over time. Statistical analyses of bead trajectories and confocal microscopy showed inter-connecting micron scale channels that penetrate throughout the biofilm, which may be important for nutrient transfer through the system. This methodology provides significant insight into a particular biofilm system and can be applied to many others to provide comparisons of biofilm structure. The elucidation of structure provides evidence for the permeability of biofilms to microscale objects, and the ability of a biofilm to mature and change properties over time.



Content from this work may be used under the terms of the [Creative Commons Attribution 3.0 licence](https://creativecommons.org/licenses/by/3.0/). Any further distribution of this work must maintain attribution to the author(s) and the title of the work, journal citation and DOI.

 Online supplementary data available from stacks.iop.org/NJP/16/085014/mmedia

Keywords: biofilms, particle tracking, biomaterials

1. Introduction

Biofilms are formed by single-cell microorganisms that adhere to a surface, aggregate, and mature, while surrounding themselves with extracellular polymeric substance (EPS), a secreted mixture of polymers consisting mainly of polysaccharides [1]. The EPS contains nucleic acids, lipids, and proteins in addition to polysaccharides, and takes up to 90% of the dry weight of the biofilm [2]. In the healthcare setting, biofilms are associated with a multitude of disease states, such as contamination of medical devices, endocarditis, and chronic infection of patients with cystic fibrosis [3]. These infections are particularly dangerous as biofilms are known to be resistant to antimicrobials, for example by decreased antimicrobial penetration through the biofilm gel matrix, or due to lower bacterial growth rates within biofilms [1]. In industrial settings, biofilms foul membrane reactors and form on ship hulls, increasing fuel expenditure.

The desire to remove biofilms from surfaces has resulted in multiple studies to understand their physical properties, including the use of standard rheometers [4–9], microfluidics devices [10–14], atomic force microscopy (AFM)/micromanipulation [15–21], or combinations thereof [22]. These techniques have been used to assess changes in biofilm properties in response to various stressors or environmental conditions. However, these techniques all provide insight into bulk, averaged physical properties rather than yielding three-dimensional (3D) details of biofilm architecture that may influence physical properties in the native biofilm state. Further, *ex situ* approaches are often invasive and do not provide insight into dynamic changes over time. Some of the rheometry and AFM technologies require scraping of a biofilm to load a test chamber, thereby destroying its internal structure, though methods have been developed for *in situ* use of these tools [4, 15, 21]. The physical properties measured by these methods span several orders of magnitude due to differences in methodology, bacterial strains, and growth conditions.

Due to heterogeneity in EPS composition and structure within a biofilm, it is important to probe localized microscale properties. The use of single particle tracking thus provides an alternative to bulk measurements by examining physical properties at the microscale with high spatiotemporal resolution [23]. Single particle tracking was first used to study the properties of reconstituted EPS, derived from purifying polysaccharides from mature biofilms [24]. Recently, a single particle tracking method was applied *in situ* to determine apparent diffusion constants of differently charged beads through biofilm, providing evidence that surface modification greatly affects mobility [25]. Bacterial tracking methods have also been employed to study the motion of flagellated and non-flagellated bacteria within biofilms, with the bacteria serving as probes for determining mechanical properties [26]. Carboxylated magnetic bead probes have been actively manipulated within *Escherichia coli* biofilms to show spatially-dependent physical properties and the effects of environment and mutations on these properties [27]. This group showed that creep compliance increased with increasing height from the bottom of a biofilm when using carboxylated magnetic microparticles as probes, indicating a stiffer matrix near the bottom of the biofilms.

While each of these methods provides insight into biofilm structures, they do not yield a comprehensive view of an *in situ* biofilm. Thus, a single particle tracking methodology is presented here that combines several techniques and analysis methods to provide a platform for studying a native biofilm's physical properties and structures. While particle tracking is a very useful technique, it is important to recognize the complexities of interpreting data measured from a living system. Multiple groups using particle tracking to study biological materials have shown that surface properties of the probes used greatly affect the measured physical properties of the material [28–31]. In particular, surface interactions due to electrostatics or hydrophobicity alter the motions of beads of the same size, resulting in different mobilities, an indication that the beads probe both sterics and chemistry of the materials of interest. These differences must be studied in order to appropriately interpret particle tracking data acquired from such biological materials. Past work on diffusion through biofilms has shown that in other bacterial species, including *Pseudomonas aeruginosa*, *Burkholderia multivorans*, and *Alteromonas macleodii*, surface charge affects the mobility of microbeads [25, 32]. Diffusion experiments on multiple species have shown that the charge of small molecules affects their ability to move through a biofilm [33]. By using multiple techniques and maintaining awareness of the complexities of the living system, the work described here probed the spatial heterogeneity of EPS, using single particle tracking to provide new information on biofilm architecture.

2. Materials and methods

2.1. Preparation of *E. coli* cultures

E. coli EMG2 [34] was used to inoculate 3 ml of lysogeny broth (LB) medium and grown on a shaker plate for 24 h at 37 °C to reach stationary phase. 100 μ l of the stationary phase culture was used to inoculate 3 ml of fresh LB, and grown at 37 °C with shaking to reach exponential phase. The culture was diluted in LB to 0.05 OD₆₀₀ from an original OD₆₀₀ between 1 and 1.5. The diluted culture was added to preformed wells constructed of PDMS bonded to a glass slide, with wells having a circular surface area, 4 mm in diameter. The cultures were grown at 37 °C, without agitation, to allow for biofilm formation. Cultures grown for two days would be left undisturbed until used for experiments. For four day cultures, LB was pipetted onto the cultures at two days to dilute any waste products released by the bacteria and provide nutrients. Fluorescent *E. coli* EMG2 harboring a protein expression plasmid (pBBR1-MCS5-*gfp*) were cultured using a similar method, but grown in LB with 0.05 μ g ml⁻¹ of gentamicin (Sigma) to maintain the plasmid.

2.2. Addition of beads to biofilms

Beads were either added to the diluted bacterial culture before placement into growth chambers or after biofilm formation. Bead stock solution diluted directly into the culture solution was added in 0.05 v/v% or less. Bead stock solution added to the biofilm after growth was diluted either 1 v/v% or 10 v/v% in LB medium, and 40 μ l of solution were gently pipetted onto the biofilm culture to avoid structural disturbance. Each type of experiment was performed in triplicate. Carboxylated beads (red and yellow-green) and aminated beads (yellow-green) were purchased from Invitrogen and Polysciences. PEGylated beads were made by conjugating

methoxy-PEG to the carboxylated beads as described previously [35]. Zeta potentials of beads suspended in LB were measured using a Malvern Zetasizer (Malvern).

2.3. Imaging of beads and analysis of motion

For bead tracking, the biofilms were imaged using an Andor iXon3-885 EMCCD camera (Andor USA) connected to an inverted fluorescence microscope (Zeiss) with a 63x oil objective (NA 1.4) to produce videos at a frame rate of 34.2 Hz with a shutter speed of 0.008 s. Three-minute long videos were taken at multiple points at the same height in the biofilm (as measured from the location of the glass slide), and the data from these multiples were grouped together when analyzing a single biofilm. Locations for videos were chosen near the center of the biofilm to avoid any edge effects that might alter physical properties. Z-stack images of biofilms with beads were captured using a Zeiss LSM 510 Meta confocal microscope (Zeiss).

Particle trajectories were determined from videos using publicly available Matlab codes (Kilfoil Group, <http://people.umass.edu/kilfoil/downloads.html>) with slight modification. Original Matlab code was used for determining two-dimensional mean-square displacements (MSD) and all other post-processing of particle trajectories. The mean-square displacement is represented as follows:

$$\text{MSD} = \langle \Delta r^2(\tau) \rangle = \langle [r(t + \tau) - r(t)]^2 \rangle, \quad (1)$$

where r represents the position of a particle, t is time, and τ is a lag time. This does not account for static error in the measurement, that is the motion that would be perceived even for static beads embedded in a solid medium [36]. To correct for this, a previously described method [37] was used to measure the MSD of beads embedded in 3% agarose, assumed to be static, and this error ($\approx 10^{-4} \mu\text{m}^2$) was subtracted to arrive at the final MSDs presented.

Calculated two-dimensional MSDs can be used to calculate creep compliance, the ratio of displacement to a given applied force over time [38]:

$$J(\tau) = \frac{3\pi d}{4k_B T} \langle \Delta r^2(\tau) \rangle, \quad (2)$$

where J represents creep compliance, d is the diameter of the probe used, T is temperature and k_B is the Boltzmann constant. Creep compliance is a material property describing deformability that should not depend on probe size assuming the probes are experiencing a homogeneous fluid, which in a gel such as biofilms means that the pore size is smaller than the probe. Given the above equation for creep compliance, scaling MSDs by bead diameter provides an indication of whether a fluid seems homogeneous at the probed length scales, and thus all graphs are presented with this scaling. As will be presented later, many of the data acquired for this system do not indicate a fluid homogenous on the probed length scales, so the value of creep compliance itself was not calculated since in this case it would not represent the actual value of the material property. The conversion between the measured scaled MSDs and creep compliance is provided in the supplementary data (available from stacks.iop.org/NJP/16/085014/mmedia).

Table 1. Properties of the surface-functionalized polystyrene microbeads used to probe biofilms. Zeta potentials are in LB medium.

Bead type	Size (nm)	Zeta potential (mV)
PEGylated	1110 ± 46	-0.3 ± 0.5
PEGylated	2020 ± 16	-2.6 ± 0.5
Carboxylated	516 ± 11	-17.7 ± 1.3
Carboxylated	1100 ± 35	-16.1 ± 0.9
Carboxylated	2000 ± 40	-28.3 ± 1.8
Aminated	1100 ± 35	-11.3 ± 0.3

3. Results and discussion

3.1. Bead motion is dependent upon surface charge

Biofilm EPS is formed from polysaccharides, proteins, lipids and DNA in water, and thus contains multiple types of charged moieties. It is therefore important to understand if surface functionalization of microbead probes plays a role in the mobility of beads in *E. coli* as the charged groups may interact with the charged portions of the matrix as they do in other biological systems. To determine if bead motion is dependent upon electrostatic interactions, the motions of 1 μm aminated, carboxylated and PEGylated beads were observed. LB medium has a Debye length of less than 1 nm (see calculation in supplementary data), and thus differences between each bead type will depend on their interactions with local charged structures. The zeta potentials of the beads in LB medium (table 1), indicate that the PEGylated beads are neutral, the carboxylated beads are negatively charged, and the aminated beads are negatively charged, with 70% of the negative charge of the carboxylated beads. PEGylated beads are considered to be generally biologically inert [39], presumably engaging in limited non-steric interactions with the biofilm. Beads 1 μm in diameter were added to bacteria solutions before biofilm formation ('pre-embedded') and after two days their motion was observed using the described protocol.

Bead motion was observed at three different heights in the biofilm (10, 20 and 30 μm above the glass slide, in a biofilm about 100 μm high—figure 1(a)). Figure 1(b) shows the scaled MSDs of the 1 μm aminated, carboxylated and PEGylated beads at 20 μm , and figure 1(c) shows the scaled MSDs at all heights at which MSDs were measured. The PEGylated beads exhibited greater mobility than both the carboxylated and aminated beads at all locations in the biofilm. In addition, at all heights the carboxylated beads were more mobile than the aminated beads, so the mobility of the beads is not monotonic with zeta potential. The carboxylated beads contain only negative surface charge, whereas the aminated beads likely contain a mix of negative and positive surface charges as they are constructed by linking amines to carboxylated beads. Biofilms contain a mix of positively and negatively charged species, but contain more anionic species, so the mixed surface charge beads can likely form more ionic interactions leading to greater confinement [2, 40, 41]. Charge interactions are therefore important when examining motion of probes within *E. coli* biofilms, and must be considered in addition to spatial confinements. While it is not certain that hydrophobic interactions play a role in the differences between bead motions, the polysaccharides that form the bulk of biofilm matrix are not known to have large hydrophobic domains. In addition, while not all the proteins within the biofilm have been characterized, the *E. coli* strain used does not produce proteins

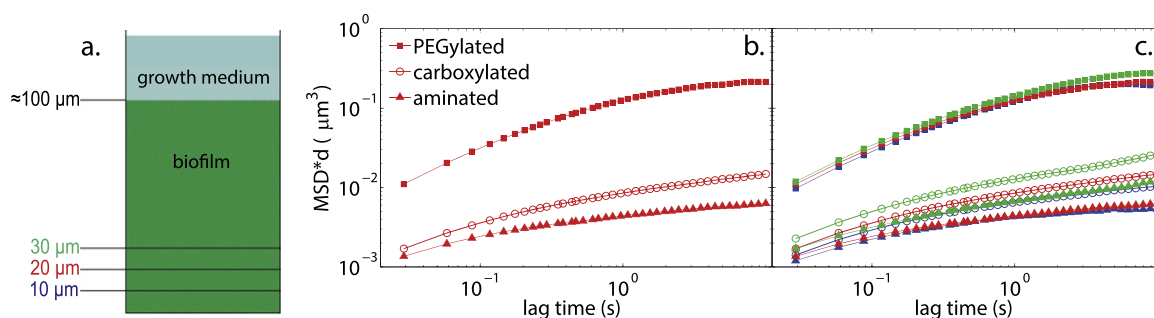


Figure 1. Bead motion in biofilms is dependent upon surface functionalization as shown by the motions of beads of the same size ($1\ \mu\text{m}$ in diameter), but different charges. (a) A schematic diagram of the biofilm showing the three heights at which MSDs were measured. Color labels (blue, red and green) are defined for each height which are used to label data in panels (b) and (c). (b) MSD versus lag time for the beads at the $20\ \mu\text{m}$ height. The PEGylated (neutral) beads were the most mobile, followed by carboxylated (negatively charged) and aminated (less negatively charged) beads. These data indicate that any confinement seen with charged beads is not necessarily due to mesh size alone, as if this were the case the three curves would be similar. (c) MSD versus lag time at 10, 20 and $30\ \mu\text{m}$ above the bottom of the biofilm, represented by blue, red, and green lines respectively. Symbols are the same as in (b) and colors defined in (a) denote the height at which the measurement was taken.

known to contribute to hydrophobicity in biofilms [42–45]. Thus, the differences seen in bead motion between the different surface charges are likely due to ionic rather than hydrophobic interactions.

3.2. Biological material accumulates over time in biofilms

PEGylated beads exhibit few interactions with biological materials [39, 46, 47] and are charge neutral so their motion in the biofilm is likely dependent primarily on steric confinement. Studying the motion of PEGylated beads embedded within a biofilm thus provides a measure of how much solid material surrounds the beads, and if this changes over the course of biofilm development. The MSDs of 1 and $2\ \mu\text{m}$ PEGylated beads embedded in biofilms were measured at two and four days of growth (figures 2(a) and (b) respectively). As shown in figure 2, the motion of PEGylated beads embedded in biofilms was found to be size dependent at both two and four days of growth. These results suggest that the PEGylated beads of different sizes experience unique microenvironments, perhaps the result of biological materials forming around the PEGylated beads with which they do not interact. The motion is not location dependent, which indicates that the mode of confinement is similar throughout the probed areas of the biofilm for each bead size.

Mobility of beads in a four day biofilm was reduced as compared to a two day old biofilm (figures 2(a), (b)), though again the motion is size but not location dependent. PEGylated beads are presumably experiencing steric confinement, so any decrease in mobility can be attributed to increased crowding of the probes by biological materials. The increased confinement observed is likely due to the accumulation of biological material from bacterial multiplication and/or release of additional EPS components as no solid materials are externally introduced into the biofilm over its growth period.

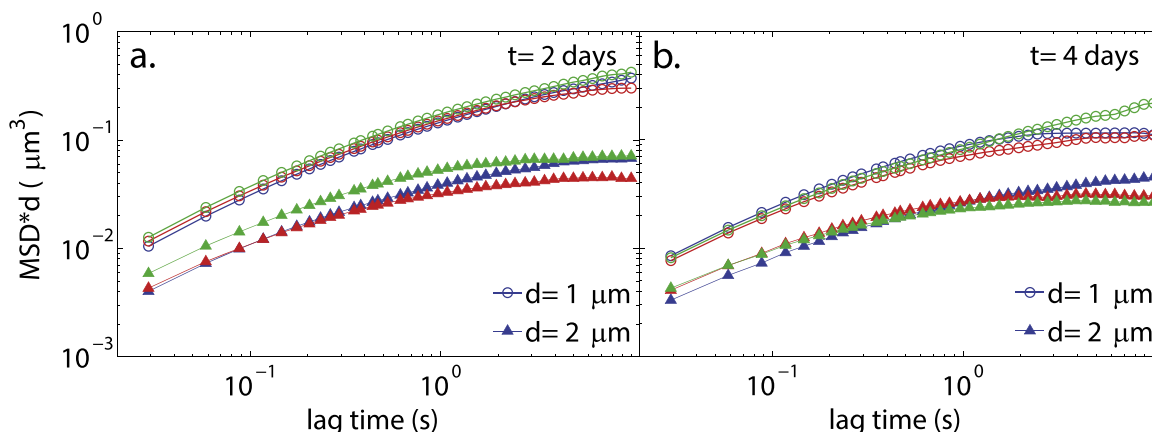


Figure 2. The motion of PEGylated beads in biofilms is size dependent at both (a) two and (b) four days. This indicates that the beads are experiencing different microenvironments, potentially due to the biological materials of the biofilm growing around the beads, as biological materials interact very little with the polyethylene glycol coating of the beads. The decrease in MSD with biofilm age with the PEGylated beads indicates that they are experiencing increased steric confinement likely due to an accumulation of biological materials, resulting in smaller regions for the beads to move in. The blue, red and green symbols represent heights of 10, 20 and 30 μm above the bottom of the biofilm respectively.

3.3. Charge density in biofilms is spatially heterogeneous, with higher density near the substrate

By measuring the motions of carboxylated beads (the base bead on which the other types are constructed) in addition to PEGylated beads, it is possible to distinguish between charge-dependent and steric interactions, and to determine which ones are impacting measured materials properties. This is important as recent work has indicated that in *Staphylococcus epidermidis*, viscoelasticity is likely mediated by self-interactions between various components of the EPS, rather than entanglements of the polysaccharides due to topological constraints [48].

If the microbead probes in a gel mesh are experiencing a homogeneous environment, then the MSDs scaled by diameter should collapse onto each other. The scaled MSD curves for carboxylated beads 0.5 and 1 μm in diameter in a two day old biofilm overlap each other at each location, which would seem to indicate that the biofilm is homogenous on this length scale at each height (figure 3(a)). If this result was due to EPS pore size alone, then larger probes would have similar MSDs. However, when the scaled MSDs for 1 and 2 μm diameter beads are compared at two days, they do not collapse onto each other (figure 3(b)). The MSDs for the 2 μm beads are larger than for the 1 μm beads, indicating that they are less confined (figure 3(b)). At four days the pattern changes and the 1 and 2 μm bead curves are closer to overlapping (figure 3(c)). This pattern of behavior would not be expected if the smaller beads are confined sterically. The strong dependence of mobility on charge suggests the confinement of carboxylated beads in *E. coli* biofilms is due to interactions with charged portions of the EPS matrix. The higher MSDs for the larger beads at two days could then be the result of the inability of the charge density at that age to arrest the motion of these beads to the same extent as the smaller beads. The height dependence of MSDs indicates that the charge density decreases at higher parts of the biofilm, either due to changes in pH of the surrounding medium

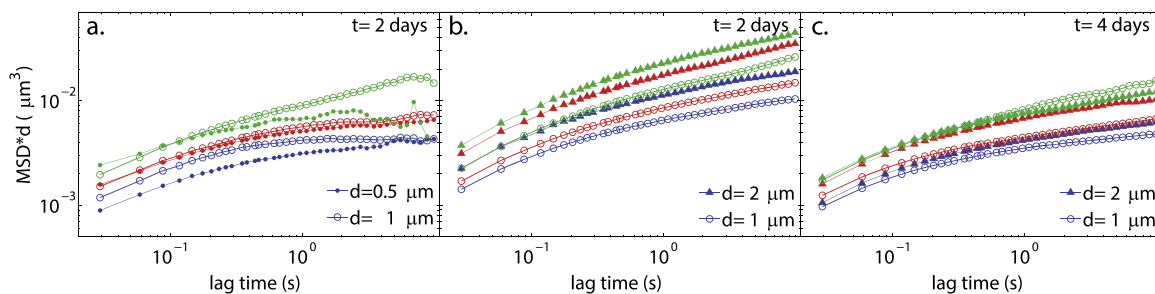


Figure 3. The motion of carboxylated beads within *Escherichia coli* biofilms. (a) Carboxylated beads 0.5 and 1 μm in diameter in a two day old biofilm have MSD curves that collapse on each other at each height when scaled by bead size. (b) Beads 1 and 2 μm in diameter do not show similar scaled MSDs at each height at two days, and counterintuitively, the MSDs for the larger beads are bigger, indicating that they are more mobile. (c) At four days, the MSD curves for the 1 and 2 μm beads get closer to overlapping at each height, indicating that the beads are getting closer to both experiencing a homogenous environment. Neither set of curves resembles those produced by beads confined due to sterics alone, as seen with PEGylated beads. The beads are thus confined by charge interactions, which are height dependent, and not strong enough at two days to restrict a 2 μm bead to the same extent as the smaller beads. The increased confinement of the largest beads at four days of growth indicates that there is an increase in charge density over time, perhaps due to bacterial secretion of additional biological materials. The blue, red and green lines represent heights of 10, 20 and 30 μm above the bottom of the biofilm, respectively.

from bacterial metabolism or the presence of different types or amounts of EPS components. The change between two and four days corroborates the prior conclusion that EPS materials are being released over time into the biofilm, and could also be due in part to changes in localized pH over time. Alternatively, the charged beads may be binding to released bacterial products, which would change their surface properties over time, resulting in the different patterns of motion at different times. However, the PEGylated beads would not experience such interactions, indicating that the addition of material to the biofilm must play some role in the altered dynamics. The biofilm is therefore actively developing over time.

3.4. Biofilms contain micron-scale, fluid-filled channels

Biofilms are known to be heterogeneous based on chemical gradients [49, 50], but their mechanical heterogeneity is not well understood. The presence of channels and voids to facilitate transport in biofilms has been suggested for several types of biofilms, based on visualizations of channels tens of microns in diameter with dye or microbeads [51, 52]. Some of these channels penetrate through biofilms, whereas others are spaces between the stalks of mushroom shaped biofilm colonies. To date, there has been no direct comparison of probe motion within various regions of the EPS to provide evidence that channels with properties distinct from that of the gel penetrate the biofilm. To provide such a comparison, beads were added onto an already-developed biofilm in order to compare their motions to those of beads pre-embedded in a biofilm. By using both measurements on the same system, it is possible to understand if channels are present, and if they are intrinsic to the system itself.

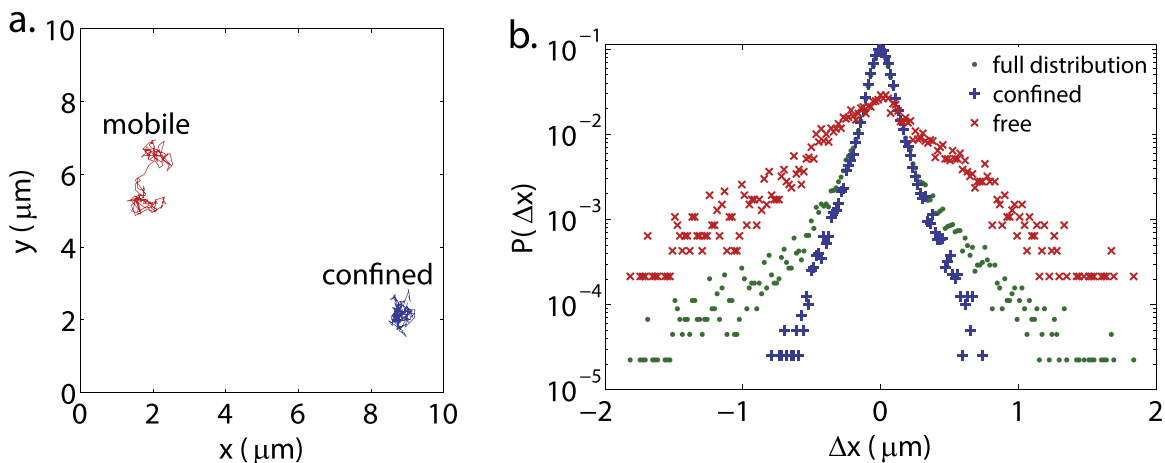


Figure 4. (a) Adding $0.5\ \mu\text{m}$ diameter carboxylated beads onto a two day old biofilm qualitatively yielded two types of bead trajectories—some that seem mobile and others that seemed confined to a particular location within the biofilm. In this image, the mobile trajectory is 4.9 s long, whereas the confined trajectory is 5.6 s long. (b) The van Hove distribution for all the beads, shown with the distribution for the statistically separated confined and free distributions at 1 s of lag time. At small Δx , the confined distribution envelopes the full distribution, whereas at larger Δx , the free distribution envelopes the full distribution. The two distinct populations indicate beads that are experiencing two different complex fluids, likely some within channels and others associated with the EPS.

A linear fit of the MSD data for pre-embedded $0.5\ \mu\text{m}$ beads (seen in figure 3(a)) at short lag times to approximate an apparent diffusion coefficient yields $D_a \approx 0.01\ \mu\text{m}^2\ \text{s}^{-1}$. Based on confocal images of the biofilms, they are approximately $100\ \mu\text{m}$ in height, which means that a lower bound on the time it would take for beads added on to a biofilm to travel through the biofilm matrix itself and reach the bottom surface would be about 12 days. However, when the beads were added onto an already grown biofilm, a concentration front reached the bottom surface on the order of hours, indicating that the beads must be traveling through something other than the dense EPS matrix probed by the pre-embedded beads. If beads were to travel through straight, water-filled channels into the biofilms, where $D \approx 1\ \mu\text{m}^2\ \text{s}^{-1}$ then the time for the concentration front to reach the bottom of the biofilm would be about 3 h, which is much closer to observed time. This indicates that the beads are likely passing through fluid-filled channels that penetrate the EPS matrix.

Qualitatively, videos of the $0.5\ \mu\text{m}$ carboxylated beads added onto a grown biofilm seemed to contain two populations of beads, some mobile, and some that seemed confined within the matrix (figure 4(a)). To determine if these were actually two separate groups, the self-portion of the van Hove correlation was calculated. This correlation measures the probability that a particle is at a position x at a given lag time ($x(\tau) = x$), assuming that a particle was at position 0 at time 0 ($x(0) = 0$), which is shown graphically by plotting the probability distribution of the step sizes made by the tracked particles for a given lag time (figure 4(b)). If the particles are undergoing Brownian motion in a homogeneous fluid, then the van Hove distribution should be a Gaussian. However, for the raw data, this distribution is clearly not a Gaussian, given its sharp central peak (figure 4(b)). A previously described unbiased statistical method [53] was used to separate the beads into two populations (mobile versus confined). In short, the range and

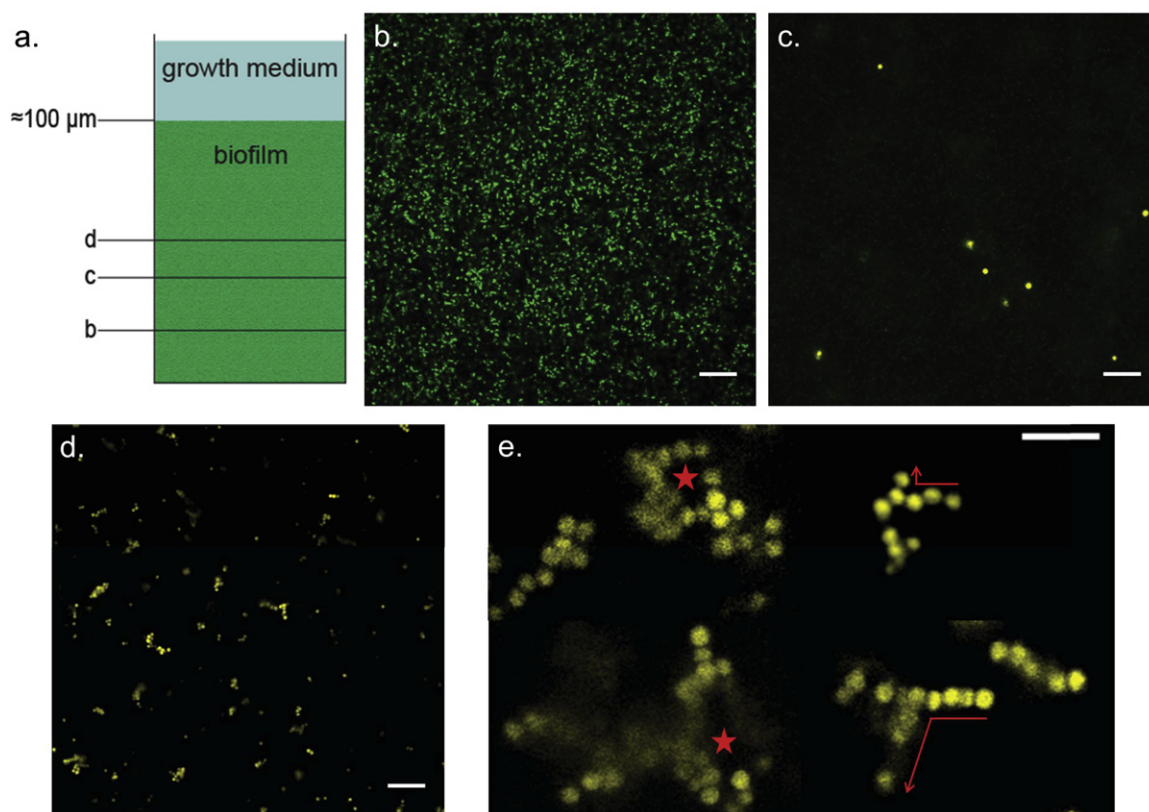


Figure 5. Confocal microscopy of fluorescent biofilms with $2\ \mu\text{m}$ beads added after growth show the following characteristic regions after 5 h. (a) Schematic diagram of image locations. (b) From $0\text{--}30\ \mu\text{m}$ from the glass surface, only bacteria are seen in the biofilm. (c) From 30 to about $50\ \mu\text{m}$ above the coverslip, many bacteria and a few lone beads are seen. (d) Above the bacteria are branched bead aggregates, with few to no surrounding bacteria. These aggregates continue higher but were not visible past $80\ \mu\text{m}$ due to objective working distance. (e) Close up view of selected aggregates, which show long, branched chains (red arrows) and some keyhole shapes (red stars in center). In all panels, the bacteria are colored green and beads are colored yellow. Scale bars are all $20\ \mu\text{m}$.

standard deviation of each individual particle trajectory were multiplied together to produce a measure of particle mobility, and an approximate cutoff for this value was determined to separate the two groups, with the beads associated with values above the cutoff identified as mobile. In this case, the cutoff chosen is $0.2\ \mu\text{m}^2$. The two populations of beads formed distinct distributions, which envelope the inner and outer regions of the combined distribution (figure 4(b)). This is an indication that the beads are in two different materials, likely fluid-filled channels and the EPS matrix. The confined beads likely correlate to beads associated with the EPS matrix, indicating that the interaction with the matrix has occurred over the experimental time scale.

Carboxylated and PEGylated beads 0.5 and $1\ \mu\text{m}$ in diameter both diffuse through biofilms on the order of hours. However, when larger, $2\ \mu\text{m}$ diameter beads were added to biofilms, few to no beads were seen at the bottom. Z-stacks acquired using confocal microscopy showed that for the first $40\text{--}50\ \mu\text{m}$ of biofilm height over the growth surface there were few to no beads and

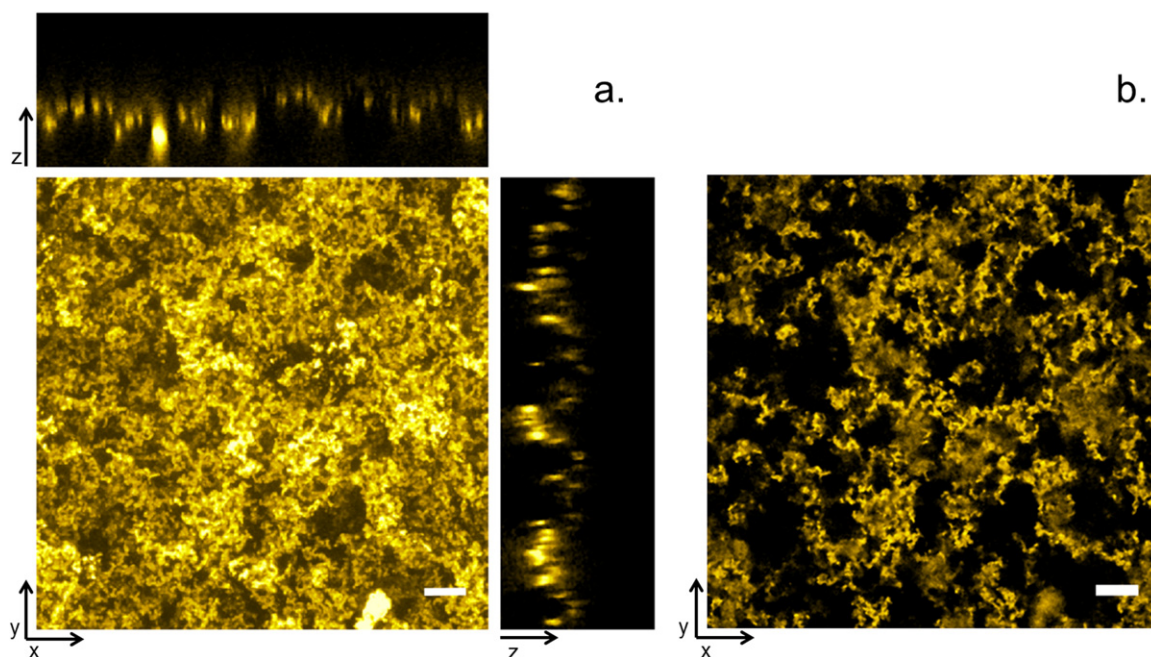


Figure 6. These are images of a biofilm 24 h after the addition of a high concentration of $0.5\ \mu\text{m}$ diameter beads to the culture. (a) Projection of a z-stack in the z direction. If one were to lie on the slide on which the biofilm was grown and look up, this is what would be seen. The brighter regions indicate what is closer to the bottom, so it is clear that there are a few branches that reach the bottom of the biofilm, and that further up there is a high density of intersecting channels. The top and side bars show the side-view in the x and y planes, respectively. These also show some regions of deeply penetrating channels and a non-uniform top surface. Each of the side views is $73.5\ \mu\text{m}$ in height. (b) An individual z-slice, about $50\ \mu\text{m}$ from the bottom of the biofilm. This shows a single plane of intersecting channels. All scale bars are $20\ \mu\text{m}$.

densely packed bacteria (figures 5(a)–(c)). Above $40\ \mu\text{m}$, long, branched clumps of $2\ \mu\text{m}$ beads were observed. These bead formations were relatively static and formed multiple types of shapes including keyhole-like structures (figures 5(a), (d)–(e)). The lack of bacteria in this region indicates that the beads are surrounded by EPS, and the long, branched structures are indicative of beads getting stuck in channels that are too small for them to get through, providing visual evidence for the channels that could transport smaller beads through the biofilms. To more clearly image the proposed channels, highly concentrated solutions of $0.5\ \mu\text{m}$ diameter carboxylated beads were added onto already grown biofilms, and allowed to diffuse through for 24 h. After 24 h, the biofilms were imaged, which revealed beads in highly branched channel-like formations (figure 6). There were fewer channels near the bottom surface of the biofilm, and a dense network at higher spatial locations, as seen in the projection of the 3D stack (figure 6(a)). A sample of a particular location, $50\ \mu\text{m}$ above the bottom of a biofilm, shows channel-like structures that connect to the planes above and below (figure 6(b)).

4. Conclusion

By combining single particle tracking, statistics, and confocal microscopy to analyze a single biofilm system, multiple structural features were elucidated. *E. coli* form biofilms with height-dependent charge density that changes with time. The physical density of the biofilm also increases with time, indicating a metabolically active system. Finally, channels exist that run through the biofilms, allowing for the passage of small molecules and micron-scale objects while limiting passage of larger objects. The wide range of features probed with this methodology makes it a useful tool for analyzing other biofilm systems, in particular for comparison of native and mutant species to determine how genetic changes influence structure formation.

Acknowledgements

This research was supported by the National Research Foundation Singapore through the Singapore MIT Alliance for Research and Technology's research program in BioSystems and Micromechanics, the National Science Foundation (CBET- 1335938), and the Cystic Fibrosis Foundation (HANES07XX0). This project was funded in part by the Charles E Reed Faculty Initiative Funds, and the Burroughs Wellcome Fund Preterm Birth Research Grant to KR. AB acknowledges support from the Hugh Hampton Young Memorial Fellowship and NIH- NIAID F30 Fellowship 1F30AI110053-01. NB acknowledges support from NIH-NIEHS Training Grant in Toxicology 5 T32 ES7020-37.

References

- [1] Hall-Stoodley L, Costerton J W and Stoodley P 2004 *Nat. Rev. Microbiol.* **2** 95–108
- [2] Flemming H C and Wingender J 2010 *Nat. Rev. Microbiol.* **8** 623–33
- [3] Donlan R M and Costerton J W 2002 *Clin. Microbiol. Rev.* **15** 167–93
- [4] Pavlovsky L, Younger J G and Solomon M J 2013 *Soft Matter* **9** 122–31
- [5] Lieleg O, Caldara M, Baumgartel R and Ribbeck K 2011 *Soft Matter* **7** 3307–14
- [6] Towler B W, Rupp C J, Cunningham A B and Stoodley P 2003 *Biofouling* **19** 279–85
- [7] Jones W L, Sutton M P, McKittrick L and Stewart P S 2011 *Biofouling* **27** 207–15
- [8] Korstgens V, Flemming H C, Wingender J and Borchard W 2001 *J. Microbiol. Methods* **46** 9–17
- [9] Houari A, Picard J, Habarou H, Galas L, Vaudry H, Heim V and Di Martino P 2008 *Biofouling* **24** 235–40
- [10] Hohne D N, Younger J G and Solomon M J 2009 *Langmuir* **25** 7743–51
- [11] Stoodley P, Lewandowski Z, Boyle J D and Lappin-Scott H M 1999 *Biotechnol. Bioeng.* **65** 83–92
- [12] Dunsmore B C, Jacobsen A, Hall-Stoodley L, Bass C J, Lappin-Scott H M and Stoodley P 2002 *J. Ind. Microbiol. Biotechnol.* **29** 347–53
- [13] Klapper I, Rupp C J, Cargo R, Purvedorj B and Stoodley P 2002 *Biotechnol. Bioeng.* **80** 289–96
- [14] Stoodley P, Cargo R, Rupp C J, Wilson S and Klapper I 2002 *J. Ind. Microbiol. Biotechnol.* **29** 361–7
- [15] Lau P C Y, Dutcher J R, Beveridge T J and Lam J S 2009 *Biophys. J.* **96** 2935–48
- [16] Aggarwal S, Poppele E H and Hozalski R M 2010 *Biotechnol. Bioeng.* **105** 924–34
- [17] Cense A W, Peeters E A G, Gottenbos B, Baaijens F P T, Nuijs A M and van Dongen M E H 2006 *J. Microbiol. Methods* **67** 463–72
- [18] Ahimou F, Semmens M J, Novak P J and Haugstad G 2007 *Appl. Environ. Microbiol.* **73** 2897–904
- [19] Aggarwal S and Hozalski R M 2010 *Biofouling* **26** 479–86
- [20] Chen M J, Zhang Z and Bott T R 2005 *Colloids Surf. B* **43** 61–71

- [21] Mosier A P, Kaloyeros A E and Cady N C 2012 *J. Microbiol. Methods* **91** 198–204
- [22] Powell L C, Sowedan A, Khan S, Wright C J, Hawkins K, Onsøyen E, Myrvold R, Hill K E and Thomas D W 2013 *Biofouling* **29** 413–21
- [23] Squires T M and Mason T G 2010 *Annu. Rev. Fluid Mech.* **42** 413–38
- [24] Cheong F C, Duarte S, Lee S H and Grier D G 2009 *Rheol. Acta* **48** 109–15
- [25] Forier K *et al* 2013 *Nanomedicine (Lond)* **8** 935–49
- [26] Rogers S S, van der Walle C and Waigh T A 2008 *Langmuir* **24** 13549–55
- [27] Galy O, Latour-Lambert P, Zrelli K, Ghigo J M, Beloin C and Henry N 2012 *Biophys. J.* **103** 1400–8
- [28] McGrath J L, Hartwig J H and Kuo S C 2000 *Biophys. J.* **79** 3258–66
- [29] Valentine M T, Perlman Z E, Gardel M L, Shin J H, Matsudaira P, Mitchison T J and Weitz D A 2004 *Biophys. J.* **86** 4004–14
- [30] Lieleg O, Vladescu I and Ribbeck K 2010 *Biophys. J.* **98** 1782–9
- [31] Xu Q, Boylan N J, Suk J S, Wang Y-Y, Nance E A, Yang J-C, McDonnell P J, Cone R A, Duh E J and Hanes J 2013 *J. Controlled Release* **167** 76–84
- [32] Nevius B A, Chen Y P, Ferry J L and Decho A W 2012 *Ecotoxicology* **21** 2205–13
- [33] Stewart P S 1998 *Biotechnol. Bioeng.* **59** 261–72
- [34] Bachmann B J 1972 *Bacteriol. Rev.* **36** 525–57
- [35] Nance E A, Woodworth G F, Sailor K A, Shih T-Y, Xu Q, Swaminathan G, Xiang D, Eberhart C and Hanes J 2012 *Sci. Trans. Med.* **4** 149ra119
- [36] Savin T and Doyle P S 2005 *Biophys. J.* **88** 623–38
- [37] Savin T, Spicer P T and Doyle P S 2008 *Appl. Phys. Lett.* **93** 024102
- [38] Wirtz D 2009 *Annu. Rev. Biophys.* **38** 301–26
- [39] Torchilin V P and Trubetskoy V S 1995 *Adv. Drug Delivery Rev.* **16** 141–55
- [40] van Hullebusch E, Zandvoort M and Lens P L 2003 *Rev. Environ. Sci. Biotechnol.* **2** 9–33
- [41] Beveridge T J, Makin S A, Kadurugamuwa J L and Li Z 1997 *FEMS Microbiol. Rev.* **20** 291–303
- [42] Van Houdt R and Michiels C W 2005 *Res. Microbiol.* **156** 626–33
- [43] Hayashi K *et al* 2006 *Mol. Syst. Biol.* **2** 2006.0007
- [44] Pouttu R, Westerlund-Wikstrom B, Lang H, Alsti K, Virkola R, Saarela U, Siitonen A, Kalkkinen N and Korhonen T K 2001 *J. Bacteriol* **183** 4727–36
- [45] Roux A, Beloin C and Ghigo J M 2005 *J. Bacteriol* **187** 1001–13
- [46] Ensign L M, Schneider C, Suk J S, Cone R and Hanes J 2012 *Adv. Mater.* **24** 3887–94
- [47] Wang Y-Y, Lai S K, Suk J S, Pace A, Cone R and Hanes J 2008 *Angew. Chemie Int. Ed.* **47** 9726–9
- [48] Ganesan M, Stewart E J, Szafranski J, Satorius A E, Younger J G and Solomon M J 2013 *Biomacromolecules* **14** 1474–81
- [49] Stewart P S and Franklin M J 2008 *Nat. Rev. Microbiology* **6** 199–210
- [50] Yu T and Bishop P L 2001 *Water Environ. Res.* **73** 368–73
- [51] Wilking J N, Zaburdaev V, De Volder M, Losick R, Brenner M P and Weitz D A 2013 *Proc. Natl Acad. Sci.* **110** 848–52
- [52] de Beer D, Stoodley P, Roe F and Lewandowski Z 1994 *Biotechnol. Bioeng.* **43** 1131–8
- [53] Rich J P, McKinley G H and Doyle P S 2011 *J. Rheol.* **55** 273–99